Nuclear Instruments and Methods in Physics Research A302 (1991) 522–528
North-Holland

# A multidimensional analysis of the Cherenkov images of air showers induced by very high energy γ-rays and protons

F.A. Aharonian and A.A. Chilingarian
*Yerevan Physics Institute, Alikhanian Brothers 2, 375036 Yerevan, Republic of Armenia*

A.K. Konopelko and A.V. Plyasheshnikov
*Altai State University, Dimitrov st. 66, Barnaul, 656099 USSR*

Received 13 March 1990 and in revised form 8 October 1990

A multidimensional analysis based on Bayes decision rules and nonparametric multivariate density estimation is proposed for classification of the Cherenkov light images of air showers registered by an air Cherenkov detector (ACD) with the multichannel light receiver. The differences in the angular size of the image, its orientation and position in the focal plane of the ACD and spectral composition of the Cherenkov light are used in the analysis to distinguish the showers induced by primary γ-rays from showers induced by background cosmic rays (CR). It is shown that the usage of several image parameters together with their correlations can lead to a reduction of the CR background rejection down to a few tenths of a percent while retaining about 50% of useful (γ-ray-induced) events.

## 1. Introduction

One of the most important problems of very high energy (VHE) γ-ray astronomy is related to the improvement of the air Cherenkov technique to effectively reduce the background hadron contamination (see, e.g., ref. [1]). Recent Monte Carlo simulations [2–5] have shown that the differences between Cherenkov light emission from air showers initiated by γ-rays and protons (and other nuclei of CR) are more pronounced than it was supposed earlier. These differences include a greater angular divergence of particles in the CR-initiated showers (p-showers) due to the multiple particle production processes.

The image of the p-shower is therefore broader, and the presence of penetrating particles in the p-shower makes the p-image also longer than the γ-shower image. The differences in the arrival direction cause the γ-shower images to have a characteristic radial alignment relative to the optical axis of the ACD. Finally, due to deeper penetration of the p-showers we expect an ultraviolet light excess for such showers.

The theoretical analysis of the efficiency of the discrimination against the CR background using the differences between p- and γ-shower images mentioned above has been carried out in refs. [2–5]. In particular, it was shown by Hillas [2] that for the 10-m telescope of the Whipple Observatory it is possible to reject up to 97–98% of the background events while retaining 60–70% of the useful events induced by γ-rays from the point source. However, the technique proposed in ref. [2], though using several image parameters simultaneously, is, in fact, a one-dimensional technique, as these parameters are treated separately, and the possible differences in the correlation between parameters for γ- and p-events are not taken into account. Our purpose is to investigate the possibility for an improvement of the background discrimination by using Bayesian decision rules and multivariate probability density estimation.

## 2. Simulation of the cascade development

The numerical analysis carried out in the present work is based on Monte Carlo simulations of development of air showers produced by VHE γ-rays and protons as well as the registration of the Cherenkov light flashes from such showers by a γ-ray telescope. The detailed description of the computational code used for VHE electromagnetic cascade simulations can be found in refs. [3,6]. The quark–gluon strings model [7] was used for the description of hadron and meson interactions. Some of the calculations of the two-dimen-

0168-9002/91/$03.50 

sional Cherenkov light images induced by p-showers were made using the radial scaling model proposed by Hillas [8], but comparison of the data obtained using the two models of strong interactions mentioned above showed no significant differences in the p-shower image parameters.

The data used in subsequent sections of this paper corresponds to a power-law primary energy spectrum ($d\mathfrak{I}/dE \sim E^{-\gamma}$). For γ-showers the power exponent γ was taken as 2.25 in the energy region (0.15–3.0) TeV. For p-showers $\gamma = 2.65$, $E \in (0.3\text{–}6.0)$ TeV.

In our calculations we considered air showers with impact parameters distributed uniformly in the range from 0 to 240 m. The optical axis of the γ-ray telescope was assumed to be in the vertical direction. The primary γ-ray arrival direction was assumed to be parallel to the telescope optical axis. The CR background showers were displaced isotropically within the field of view of the telescope.

The main characteristic of the simulated optical reflector camera is its effective area $S_{\text{eff}} = \eta k S \approx 10$ m$^2$ where $S$ is the geometric area, $\eta$ is the reflectivity of the mirror, and $k$ is the quantum efficiency of phototubes. The altitude was taken to be 1000 m above sea level.

Two hexagonal configurations of the multichannel light receiver were considered. The first of them (basic configuration) has 37 pixels with the angular size of each of them 0.5° and the total viewing angle 2.5°. For the second configuration the total number of pixels is 127, the pixel size is 0.25°, and the total field of view is 3.25°.

To reject random flashes from the night sky background we took into consideration (following the recommendations of the experiment [9]) only such events that give signals exceeding 80 photoelectrons (40 electrons for configuration 2) in at least two pixels of the light receiver (excepting the outer pixel ring for configuration 1 and two outer pixel rings for configuration 2). We attributed shower images having the largest signal in one of the pixel rings to so-called ZONEs which were numbered from the central pixel as 0, 1,..., 7. In the calculations of two-dimensional shower image parameters we neglected contributions from pixels having values less than 1% from the total Cherenkov light flash intensity.

In the multidimensional analysis presented here we considered a number of the shower image parameters proposed earlier in refs. [2,3,5]. They are LENGTH, WIDTH – the longitudinal and lateral sizes of the Cherenkov light spot in the focal plane of the telescope reflector; ALPHA – the angle between the main axis of the spot and the direction to the focal plane center; MISS = DIST × sin(ALPHA), where DIST is the angular distance of the image centroid from the center of the field; TH = (WIDTH × LENGTH)$^{1/2}$; AZWIDTH = WIDTH/cos(ALPHA); U/V – the ratio of the total flash intensities in ultraviolet (0.2–0.3 μm) and visible (0.3–0.6 μm) spectral regions.

## 3. Bayesian classification of Cherenkov light images

The Bayesian approach formalizes the account of all the losses connected with probable misclassification and utilizes all the differences of alternative classes [10,11]. The decision problem in a Bayesian approach is simply described in terms of the following probability measures defined on metric spaces:

(a) The space of possible states of nature – $\theta = (\text{p}, \gamma)$ where p and γ are the indexes of alternative classes (hypotheses);

(b) The space of possible statistical decisions – $\tilde{\theta} = (\tilde{\text{p}}, \tilde{\gamma})$ – the decision that the examined image is caused by a primary proton or a γ-quantum;

(c) Cost (losses) measure $C_{\theta\tilde{\theta}}$ defined on the direct product of nature states and decision spaces ($\theta \times \tilde{\theta}$). At correct classification the losses are equal to zero:

$$C_{\text{p}\tilde{\text{p}}} = C_{\gamma\tilde{\gamma}} = 0.$$

If we misclassify the signal event, we decrease the efficiency of γ-event registration. If we attribute hadronic images to γ-ray ones, we increase the background contamination. As we expect a significant excess of background against signal, we are interested in a strong background rejection. It is not therefore reasonable to take the symmetric loss function $C_{\text{p}\tilde{\gamma}} = C_{\tilde{\text{p}}\gamma} = 0.5$, as we did in our earlier studies concerning the cosmic-ray hadron classification by a transition radiation detector and iron nuclei fraction determination in the primary flux [12].

The determination of $C_{\text{p}\tilde{\gamma}}$ and $C_{\gamma\tilde{\text{p}}}$ values was done by maximization of the ratio of the signal value to the background fluctuations. By such a way we can obtain signal acceptance about 50% and a significant background rejection (greater than 99%);

(d) Event (measurement, feature) space – a set of possible results of a random experiment – image parameter samples obtained by a Monte Carlo simulation. We shall denote these samples by $\omega_{\text{p}}$ and $\omega_{\gamma}$ and call them training samples (TS), as the experimental image handling procedure parameters are determined by these samples;

(e) The prior measure $P_\theta = (P_\gamma, P_{\text{p}})$. We used for this measure the uniform distribution $P_\gamma = P_{\text{p}} = 0.5$. In this case classification results will depend only on the available experimental information and the losses. A more detailed discussion of the prior measure choice can be found in ref. [13];

(f) Conditional density (likelihood function), $\{p(x/\omega_{\text{p}}), p(x/\omega_\gamma)\}$.

Estimating the conditional (on particle type) density on the basis of a collection of simulations is a typical

problem in cosmic-ray and high-energy physics. The application of nonparametric local density estimation methods (the kernel-type Parzen estimates [14], the K-nearest-neighbors (KNN) estimates [15]) gives the best results. Our development of these nonparametric density estimates [16] makes their use in cosmic-ray physics considerably more simple and increases their precision.

Let us introduce an invariant metric in an $N$-dimensional feature space (Mahalonobis distance):

$$R_{\mathrm{Mah}} = (x' - x)^{\mathrm{T}} \Sigma^{-1} (x' - x), \tag{1}$$

where $\Sigma$ is a covariance matrix calculated by means of the TS to which $x'$ belongs and T denotes matrix transposition. Then the KNN density estimate takes the form:

$$P_K(x/\omega_{\mathrm{i}}) = \frac{K-1}{M_{\mathrm{i}} V_{\mathrm{i}}(x)}, \qquad \mathrm{i} = \mathrm{p},\ \gamma, \tag{2}$$

where $V_{\mathrm{i}}(x)$ is the volume of an $N$-dimensional sphere containing $K$ elements of the TS nearest to the point $x$; $K$ is the parameter controlling the degree of smoothing of the empirical distribution; $M_{\mathrm{i}}$ is the TS size.

As our Monte Carlo is a weighted one, we modify the KNN method to the so-called "heavy ball" method:

$$P_r(x/\omega_{\mathrm{j}}) = \sum_{i=1}^{K_{\mathrm{j}}} S_i \Big/ \sum_{i=1}^{M_{\mathrm{i}}} S_i V_r, \qquad \mathrm{j} = \mathrm{p},\ \gamma, \tag{3}$$

where $S_i$ is the event weight; $r$ is the ball radius; $V_r$ is the ball volume; $K_{\mathrm{j}}$ is the number of events falling into the ball. Here, instead of counting the number of events, the total weight of the events is calculated, and the ball radius is fixed instead of the parameter $K$. The calculations are carried out for several values of $r$ simultaneously. Then the obtained density estimates are ordered according to their magnitude and the median of the ordered sequence is taken as the final estimates;

(g) The a posteriori density $p(\omega/x) = \{ p(\omega_{\mathrm{p}}/x), p(\omega_{\gamma}/x)\}$ in which the prior and experimental information is included. As we choose a uniform prior information, the a posteriori density coincides with the conditional one.

Proceeding from the above definitions we can introduce the Bayesian decision rule:

$$P(x/\omega_{\gamma}) C_{\mathrm{p}\tilde{\gamma}} \gtrless P(x/\omega_{\mathrm{p}}) C_{\gamma\tilde{\mathrm{p}}} \rightarrow x \in \begin{cases} \gamma, \\ \mathrm{p}. \end{cases} \tag{4}$$

## 4. Selection of an optimal feature combination

The pattern recognition is a two-stage process. It includes selection of informative variables and construction of a classifier (a decision rule) performing the recognition.

The most important problem in any field is feature extraction. Though this problem can be formalized by a linear (or nonlinear) feature space transformation [17], the feature selection problem depends mostly on the experimenter's intuition.

The quantitative comparison of the distinctive information contained in one-dimensional distributions can be made by the so called $P$-values (and $\sigma_{\mathrm{P}}$ quantiles) of standard statistical tests.

$$P = \int_{\sigma_{\mathrm{P}}}^{\infty} f(x)\, \mathrm{d}x,$$

where $f(\cdot)$ is the test function (usually a standard Gaussian distribution), and $\sigma_{\mathrm{P}}$ is the test statistic, calculated by model or experimental data. $P$ equals the probability of incorrectly rejecting the null hypothesis (the hypothesis that the $\gamma$-sample and p-sample come from the same population). Thus the $P$-values are inversely proportional to the studied image parameters discriminative value. Instead of using $P$-values, which are usually very small, we shall use the $\sigma_{\mathrm{P}}$ quantile values for comparison purposes.

The Kolmogorov nonparametric test, the Student parametric test and the Mann–Whitney rank test were used for this purpose [18]. The Fisher test was used [19] to determine the significance of correlation differences. Beside that, the so-called Bhatacharia probabilistic distance was used [20].

Table 1
$\sigma_{\mathrm{P}}$-quantiles of one-dimensional tests, 37 channels, ZONE 2, $\#\gamma/\#\mathrm{p} = 584/364$

| Tests | AZWID | U/V | MISS | LENGTH | WIDTH | TH |
|---|---|---|---|---|---|---|
| Student | 24.86 | 14.37 | 31.76 | 19.04 | 6.85 | 17.08 |
| Kolmogorov | 11.35 | 7.49 | 10.79 | 8.90 | 5.54 | 8.95 |
| Mann–Whitney | 21.54 | 16.33 | 21.64 | 15.84 | 10.35 | 15.81 |
| Bhatacharia | 0.61 | 0.14 | 0.56 | 0.52 | 0.12 | 0.36 |
| Bayes error upper bound | 0.27 | 0.44 | 0.29 | 0.30 | 0.44 | 0.35 |

Table 2
Comparison of correlations between parameters of p- and γ-shower images by means of the Fisher test $P$-value, 37 channels, ZONE 2, #γ/#p = 584/364

| | AZWID | U/V | MISS | LENGTH | WIDTH | TH |
|---|---|---|---|---|---|---|
| AZWID | * | | | | | |
| U/V | 1.968 | * | | | | |
| MISS | 4.298 | 2.271 | * | | | |
| LENGTH | 18.561 | 0.735 | 0.503 | * | | |
| WIDTH | 24.814 | 6.989 | 6.985 | 3.785 | * | |
| TH | 3.102 | 4.628 | 4.559 | 8.655 | 2.974 | * |

The Bhatacharia distance consists of two parts – the difference in the mean values and in covariances:

$$R_{\mathrm{Bha}} = \tfrac{1}{8}(\mu_1-\mu_2)^T\left(\frac{\Sigma_1+\Sigma_2}{2}\right)^{-1}(\mu_1-\mu_2) + \frac{1}{2}\ln\left(\frac{\frac{1}{2}|\Sigma_1+\Sigma_2|}{|\Sigma_1|^{1/2}|\Sigma_2|^{1/2}}\right), \quad (5)$$

where $\mu_1$, $\mu_2$ are the feature mean values; $\Sigma_1$, $\Sigma_2$ are covariance matrices. The Bhatacharia distance is equal to zero if the classes completely overlap and it is equal to $\infty$ if they do not overlap at all. Through the Bhatacharia distance one can express the upper bound of the expected misclassification rate:

$$U_{\mathrm{B}} = 1 - \exp(-2R_{\mathrm{Bha}}). \quad (6)$$

In table 1 we give some results on the application of these statistical tests. The results in this table were obtained using events having the largest value of the signal magnitude in one of the pixels from the second pixel ring (ZONE 2) of the basic light receiver configuration. As can be seen from the table parameters AZWIDTH and MISS have the largest $P$-quantile values and the largest values of the probabilistic distance.

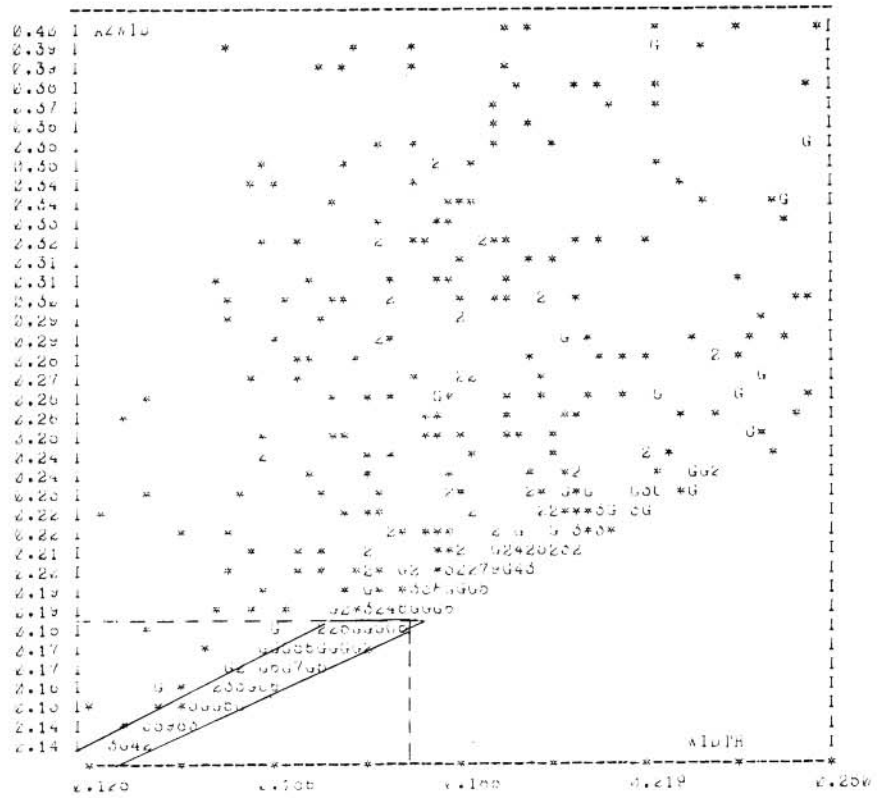

Fig. 1. Scatter plot: WIDTH vs AZWID. *: P images, 364 events, correlation 0.369. G: gamma images, 586 events, correlation 0.910.

Table 3
Probabilistic distances between parameter distributions of Cherenkov images of p- and γ-showers, 37 channels

| Distance | WIDTH AZWID | LENGTH AZWID | WIDTH LENGTH AZWID | WIDTH LENGTH AZWID U/V |
|---|---|---|---|---|
| Mahalonobis | 0.282 | 0.275 | 0.278 | 0.302 |
| Correlation | 0.812 | 0.530 | 1.046 | 1.070 |
| Bhatacharia | 1.004 | 0.805 | 1.324 | 1.431 |
| Bayes error upper bound | 0.167 | 0.224 | 0.133 | 0.120 |

Therefore, for these parameters the smallest overlapping takes place of the probability distributions corresponding to the alternative classes, and these parameters are the best ones.

The best pairs of features can be chosen by their correlation differences in alternative classes (see table 2). We can select the AZWIDTH–WIDTH pair on the basis that it yields the largest Fisher test value. Such a choice can be explained in the following way. For γ-images the correlation between AZWIDTH and WIDTH parameters is very strong ( ~ 1), because the plane-parallel direction of γ-rays arriving causes a radial alignment of patterns in the telescope focal plane, and AZWIDTH practically coincides with WIDTH. Images from isotropically distributed cosmic-ray protons have no preferable orientation, and the correlation between the these two parameters is not pronounced.

From the scatter plot of values of parameters WIDTH and AZWIDTH (fig. 1) we can see that the γ-domain chosen by a correlation analysis (polygonal region) is considerably better than that obtained in the ref. [2] (rectangular domain in the left lower corner of the plot) without taking into account correlations between WIDTH and AZWIDTH. A more complicated domain obtained from a multidimensional analysis provides much higher levels of signal acceptance and background rejection. On the other hand, the successive one-dimensional analysis ignores the correlation information and thus cannot outline the best γ-domain.

From table 3 it is seen that the "correlation" part of the Bhatacharia distance is about a factor of three larger than its "mean value difference" part. It is another confirmation that consideration of correlations is very important for the imaging technique.

Finally, the features should be selected as follows:

(a) The best single image parameters are selected by one-dimensional tests (table 1);

(b) The best pairs and triples are selected so that at least one of the parameters chosen above is included and their correlations are significantly different for the γ- and p-events (table 2).

Note that there are some restrictions on the possible space dimensionality which are based on the sample size [21] and which prevent increasing the number of parameters in the combination under investigation. For Cherenkov images we expect five independent parameters only – two for the image shape, one for orientation, one for position and one for the ultraviolet fraction (the U/V ratio).

## 5. The results of the multidimensional shower image analysis

To apply the technique developed here to shower image classification we used the so called "leave-one-out-at-a-time" test (the U-method). It has been shown in [22] that the U-method provides much lower bias than other methods.

According to the U-method, one event is removed from the TS, the training (conditional density estimate) is performed without it, then that element is classified and replaced in the TS. This procedure is repeated until all the TS elements are classified. By this the error rates $R_{\gamma\bar{p}}$ and $R_{p\bar{\gamma}}$ corresponding to the maximum available value of the signal-to-background-ratio improvement-factor,

$$\eta = \left(1 - R_{\gamma\bar{p}}\right)/\sqrt{R_{p\bar{\gamma}}}\,, \tag{7}$$

are obtained.

In table 4 we present some results of application of this technique for the case of the a parameter. In addition, we present in this table results obtained on the basis of the Monte Carlo calculations of Hillas taken from ref. [23]. It may be seen from the table that there is a good agreement between the data.

Table 4
Data on the discrimination against p-showers in the case of single discrimination parameters usage, 37 channels, ZONE1 and ZONE2

| | LENGTH | WIDTH | DIST | MISS | AZWID |
|---|---|---|---|---|---|
| Our data [a,b] | 0.932 | 0.942 | 0.791 | 0.714 | 0.615 |
| | 0.186 | 0.458 | 0.384 | 0.206 | 0.069 |
| | 2.162 | 1.392 | 1.276 | 1.571 | 2.346 |
| From ref. [23] [a] | 0.826 | 0.858 | 0.935 | 0.676 | 0.768 |
| | 0.210 | 0.367 | 0.683 | 0.231 | 0.121 |
| | 1.802 | 1.416 | 1.132 | 1.408 | 2.204 |

[a] 1st line: acception efficiency for gamma showers $R_{\gamma\bar{\gamma}}$; 2nd line: contributed proton showers background $R_{p\bar{\gamma}}$; 3rd line: discrimination efficiency improvement $R_{\gamma\bar{\gamma}}/\sqrt{R_{p\bar{\gamma}}}$.

[b] To obtain these data special calculations were done in which the same observation level and effective mirror surface square as in ref. [23] were used.

Table 5
Comparison of different parameters combinations for multidimensional proton background rejection

| ZONE | EVENT (#γ/#P) | TH LENGTH AZWID [a] | WIDTH LENGHT MISS [a] | WIDTH LENGTH AZWID [a] | WIDTH LENGTH MISS U/V [a] | WIDTH LENGTH U/V AZWID [a] | TH LENGTH U/V AZWID [a] |
|---|---|---|---|---|---|---|---|
| *37 channels* | | | | | | | |
| 1 | 639/229 | 0.421 | 0.228 | 0.333 | 0.445 | 0.346 | 0.379 |
| | | 0.016 | 0.008 | 0.008 | 0.004 | 0.003 | 0.003 |
| | | 3.320 | 2.549 | 3.674 | 6.973 | 6.317 | 6.572 |
| 2 | 584/364 | 0.537 | 0.411 | 0.501 | 0.698 | 0.51 | 0.384 |
| | | 0.001 | 0.004 | 0.001 | 0.012 | 0.001 | 0.001 |
| | | 21.820 | 6.766 | 13.077 | 6.299 | 17.652 | 11.410 |
| All | 1797/939 | 0.317 | 0.543 | 0.384 | 0.394 | 0.363 | 0.411 |
| | | 0.004 | 0.047 | 0.010 | 0.018 | 0.013 | 0.018 |
| | | 4.958 | 2.503 | 3.896 | 2.958 | 3.172 | 3.050 |
| 1 & 2 | 1233/593 | 0.477 | 0.315 | 0.414 | 0.565 | 0.429 | 0.381 |
| | | 0.007 | 0.006 | 0.004 | 0.009 | 0.002 | 0.002 |
| | | 5.689 | 4.232 | 6.806 | 6.388 | 10.210 | 9.071 |
| *127 channels* | | | | | | | |
| 3 | 336/156 | 0.605 | 0.722 | 0.584 | 0.552 | 0.654 | 0.628 |
| | | 0.003 | 0.008 | 0.002 | 0.001 | 0.002 | 0.002 |
| | | 10.770 | 8.273 | 12.120 | 15.560 | 14.624 | 14.050 |
| 4 | 345/214 | 0.624 | 0.658 | 0.649 | 0.583 | 0.624 | 0.590 |
| | | 0.004 | 0.004 | 0.004 | 0.004 | 0.004 | 0.004 |
| | | 9.448 | 9.887 | 9.834 | 8.836 | 9.449 | 8.943 |

[a] 1st line: acception efficiency for gamma showers $R_{\gamma\tilde{\gamma}}$; 2nd line: contributed proton showers background $R_{p\tilde{\gamma}}$; 3rd line: discrimination efficiency improvement $R_{\gamma\tilde{\gamma}}/\sqrt{R_{p\tilde{\gamma}}}$.

The results of multidimensional analysis for several image parameter combinations are presented in table 5. It is seen that background contamination can be rejected down to a few tenths of a percent. For the 37 channel receiver configuration with a pixel size of 0.5° the best background discrimination is attained for the second ZONE. The 127-channel camera with a pixel size of 0.25° provides almost uniform background rejection over all the central ZONEs.

It should be noted that the very large $\eta$ values in table 5 (values in excess of 10) would have large statistical uncertainty due to the limited number of background images.

As you can see in fig. 2 we can choose the value of the losses measure to obtain the desirable relation between the coefficients of the signal acceptance and background rejection. Moving to the left along the $x$ = axis of fig. 2 we can reach the almost background-free region at losses value $< 0.5$. But for small values of losses (this corresponds to low values of background contamination) the signal acceptance level will be quite high (say, about 0.5) only in the case of multidimen-

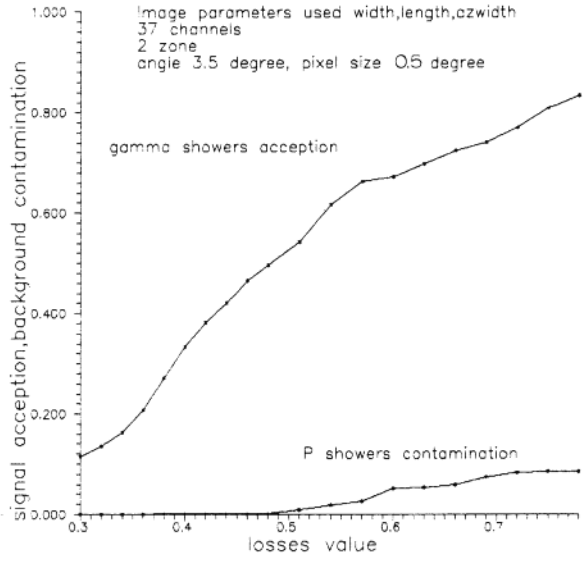


Fig. 2. Bayesian classification.

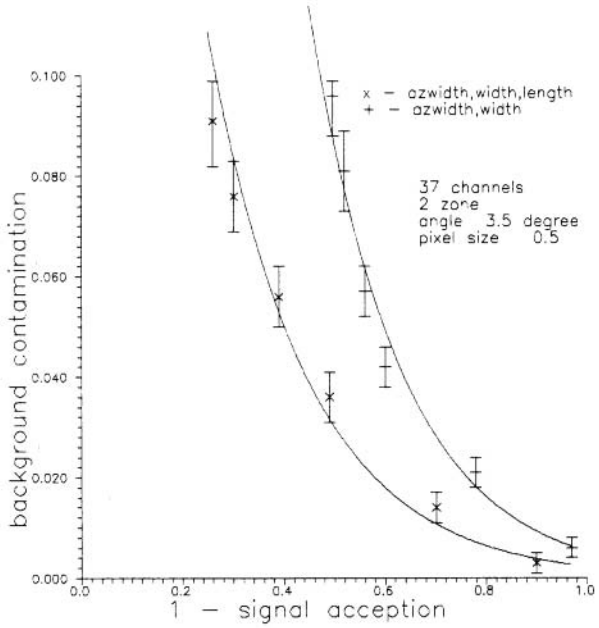


Fig. 3. Preference curves.

sional analysis. This can be seen from fig. 3 where the relations between background rejection and signal detection effectiveness are presented for parameters combinations AZWIDTH + WIDTH + LENGTH, AZWIDTH + WIDTH.

To conclude, multidimensional analysis provides much greater discrimination efficiency compared to the application of several image parameters independently without taking into account their correlations as in ref. [24].

## Acknowledgement

We are grateful to M. Cawley for useful discussions.

## References

[1] T.C. Weekes, Nucl. Instr. and Meth. A264 (1988) 55.
[2] A.M. Hillas, Proc. 19th ICRC, USA, 1985, vol. 3, p. 445.
[3] A.V. Plyasheshnikov and G.F. Bignami, Nuovo Cimento 8c (1985) p. 39
[4] T.C. Weekes, R.C. Lamb and A.M. Hillas, Proc. NATO Workshop on VHE γ-Ray Astronomy, Durham, ed. K.E. Turver (Reidel, Boston, 1987) p. 235.
[5] Y.L. Zyskin, Proc. Worksop of VHE γ-Ray Astronomy, Crimea, 1989, p. 148.
[6] A.V. Plyasheshnikov and A.K. Konopelko, The energy estimation of VHE γ by the Cerenkov teleskope with the multi-channel receiver, Proc. workshop of VHE gamma-ray astronomy, Crimea, 1989.
[7] Y.M. Shabelsky, Preprint LIAF, 1986.
[8] A.M. Hillas, Proc. 16th ICRC, Kyoto, Japan, 1979, vol. 6, p. 13.
[9] M.F. Cawley, D.J. Fegan et al., Proc. 19th ICRC, USA, 1985, vol. 3, p. 449.
[10] H. Raiffa and R. Schlaifer, Applied Statistical Decision Theory (MIT, Cambridge, MA, 1978).
[11] J.D. Hey, An Introduction to Bayesian Statistical Inference (Robertson, 1983).
[12] V.G. Denisova, A.M. Dunaevsky, S.A. Slavatinsky et al., Proc. 20th ICRC, Moscow, USSR, 1987, vol. OG 5.1, p. 390.
[13] E.E. Leamer, Ad hoc Inference with Nonexperimental Data (Wiley, New York, NY, USA, 1981).
[14] E. Parzen, Ann. Math. Stat. 33 (1962) 1065.
[15] D.O. Lofsgaarden and C.D. Quesenberry, Ann. Math. Stat. 36 (1965) 1049.
[16] A.A. Chilingarian, Comput. Phys. Commun. 54 (1989) 381.
[17] K. Fukunaga, Introducton to Statistical Pattern Recognition (Academic Press, New York, 1972).
[18] System/360 Scientific Subroutine Package (360a-cm-03x) (IBM, Technical Publications Department, New York, NY, USA, 1971).
[19] K. Uberla, Faktorenanalysis (Springer, Berlin, 1977).
[20] A. Bhatacharia, Sankhya 7 (1946) 401.
[21] S.Kh. Galfayan, A.M. Dunaevsky et al., Preprint FIAN no. 332 (1986).
[22] A.A. Chilingarian, S.Kh. Galfayan et al., Proc. 20th ICRC, Moscaw, USSR, 1987, v. HE5, p. 487.
[23] K.G. Gibbs, Ph.D. thesis, University of Arizona (1986).
[24] A.M. Hillas, J.R. Patterson, Proc. NATO Workshop on VHE γ-Ray Astronomy, Durham (Reidel, Boston, 1987) p. 249.